Boolean Network Modeling-Guided Identification of FDA-Approved Drug Combinations for Targeted Treatment Strategies in Head and Neck Cancer

Pranabesh Bhattacharjee
Department of Electrical and Computer Engineering, Texas A&M University, College Station, TX 77843, USA.
p.bhattacharjee@tamu.edu

Aniruddha Datta
Department of Electrical and Computer Engineering, Texas A&M University, College Station, TX 77843, USA.
datta@ece.tamu.edu

***Abstract*— Head and neck cancer (HNC) presents significant therapeutic challenges due to pathway redundancies and resistance mechanisms. To address this, we developed a Boolean network model integrating key signaling pathways—EGFR, Wnt, Hippo-YAP, MAPK/ERK, and PI3K/mTOR—to systematically assess single and combination drug therapies. Using the Normalized Mean Size Difference (NMSD) metric, we quantified the efficacy of targeted drugs (FDA approved or under investigation with promising efficacy) against tumors with multiple mutations.**

Our simulations identified VT3989 (YAP/TEAD inhibitor) as the most effective monotherapy. Among two-drug combinations, Ulixertinib (ERK inhibitor) and VT3989 exhibited the lowest NMSD, indicating strong synergistic inhibition of MAPK and Hippo pathways. Adding Vorinostat (FBXW7 modulator) further enhanced efficacy, achieving 80% efficacy. The most effective combination—Temsirolimus (mTOR inhibitor), Ulixertinib, VT3989, and Vorinostat—demonstrated an 88.3% improvement over untreated conditions.

Our findings support a shift from sequential to concurrent multi-pathway targeting, mirroring clinical evidence that combination approaches delay resistance. The hierarchical NMSD reductions from 0.685 (single-agent) to 0.120 (four-drug therapy) highlight the advantage of combination size in pathway control. This computational framework provides a rationale for prioritizing Temsirolimus-containing quadruple therapies, offering a novel precision oncology strategy for HNC with complex mutational landscapes.

Keywords*— *Boolean Network, Combination Therapy, Drug Repurposing, Head and Neck Cancer, Targeted Therapy, TEAD Inhibitor, Vorinostat, YAP/TEAD Inhibitor.

I. INTRODUCTION

Head and neck cancer (HNC) encompasses a diverse group of malignancies arising from the oral cavity, pharynx, and larynx and remains a significant global health concern. According to the American Cancer Society's 2025 Cancer Facts & Figures report, an estimated 71,110 new cases of HNCs will be diagnosed in the U.S. in 2024, with approximately 16,110 deaths expected [1]. This represents about 4% of all cancers in the U.S. Globally, the incidence of HNC is projected to increase by 30% annually by 2030. This rise is largely attributed to increases in oropharyngeal cancer, particularly HPV (Human Papillomavirus)-related cases in developed countries [2]. In fact, it is expected that HPV will overtake tobacco as the leading contributor to the global HNC burden in the coming years [3]. Recent trends show that HNC incidence is rising more rapidly in women, especially those under 50 years old. From 2002 to 2021, cancer incidence in women younger than 50 increased from 51% higher than men to 82% higher. This trend is particularly notable for oral cancers, with significant increases observed across all age groups, especially in older women [4] [5]. In Europe, a study using data from the Polish Cancer Register (1999-2021) revealed increasing incidence rates across different age cohorts, with the 60-69 age group showing the fastest increase, particularly for oral and oropharyngeal cancers in women. In the UK, HNC mortality rates are projected to rise by 12% between 2023-2025 and with an estimated 6,700 deaths annually by 2038-2040 [6]. Despite advances in surgical techniques, radiotherapy, and chemotherapy, the 5-year survival rate of HNC patients remains below 50%, largely due to late diagnosis, high rates of recurrence, and therapeutic resistance [7]. Current treatments are often limited by toxicity and lack of specificity, underscoring the urgent need for more precise, targeted therapeutic strategies.

Molecular studies have revealed that HNC is driven by complex dysregulations in several oncogenic pathways, including EGFR, PI3K/AKT/mTOR, RAS/RAF/MEK/ERK, JAK/STAT, Wnt/β-catenin, and Hippo-YAP/TAZ, alongside frequent mutations in tumor suppressors like p53, PTEN, and FBXW7 [8][9]. These alterations promote uncontrolled proliferation, evasion of apoptosis, angiogenesis, and metastasis. Consequently, targeting multiple pathways simultaneously through drug combinations has emerged as a promising strategy to overcome compensatory signaling and resistance mechanisms [10].

This work was supported in part by the National Science Foundation under Grant ECCS-1917166 and in part by the J. W. Runyon, Jr. 35 Professorship II funds.

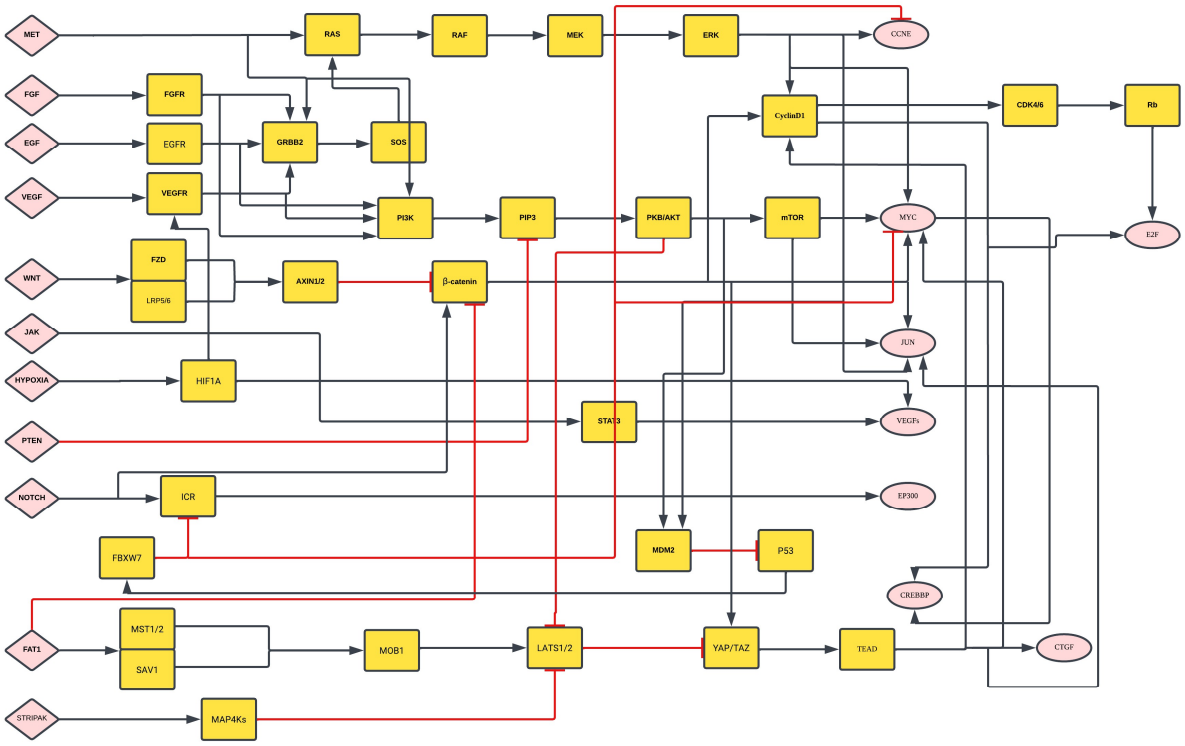

FIGURE 1. HNC signaling pathway.

In recent years, FDA-approved drugs have been increasingly investigated for repurposing in HNC, owing to their established safety profiles and expedited clinical translation. However, given the high interconnectivity and feedback within HNC signaling networks, empirically identifying effective drug combinations remains challenging [11]. Computational approaches, particularly Boolean network (BN) modeling, provide a powerful framework to simulate pathway behavior and predict cellular responses under various perturbations [12]. Boolean models, by simplifying the states of biological systems into binary ones (ON/OFF), enable the exploration of complex gene regulatory and signaling networks, making them ideal for hypothesis-driven drug discovery in cancer research.

In this study, we constructed a comprehensive BN model of HNC, integrating key components involved in tumor growth, survival, angiogenesis, and apoptosis. We systematically simulated the effects of twelve targeted drugs (FDA approved or under investigation with promising efficacy), both as monotherapies and in combination, to identify optimal therapeutic strategies that disrupt oncogenic signaling and restore tumor-suppressive functions. This network-driven approach aims to guide robust combination therapies, ultimately contributing to personalized and more effective treatments for HNC patients.

II. Overview of HNC Pathway

HNC is driven by the dysregulation of multiple interconnected signaling pathways (Fig.1) that control cell proliferation, apoptosis, angiogenesis, and immune evasion [13]. Molecular alterations, including gene mutations, amplifications, and loss of tumor suppressor functions, contribute to the aggressive progression of HNC [14]. The key oncogenic drivers and tumor suppressors identified in the constructed Boolean model of HNC are integrated into a complex network, reflecting the real tumor biology of this disease [15].

The process begins with the activation of receptor tyrosine kinases (RTKs), such as EGFR, FGFR, VEGFR, and MET. These receptors are stimulated by their respective ligands, including EGF, FGF, VEGF, and hepatocyte growth factor (HGF) [16]. Activation of these receptors initiates intracellular signaling cascades that promote proliferation and survival. One major downstream pathway activated by RTKs is the PI3K/AKT/mTOR pathway, which then activates increased protein synthesis, enhanced cell survival, and resistance to apoptosis [17]. The tumor suppressor PTEN, which normally inhibits this pathway, is frequently lost or inactivated in HNC, further amplifying PI3K/AKT signaling [18].

Parallel to PI3K signaling, RTKs also activate the RAS/RAF/MEK/ERK pathway. This cascade promotes cell cycle progression by inducing the expression of key regulators such as Cyclin D1, MYC, and JUN [19]. These transcription factors stimulate the production of proteins necessary for the G1/S transition of the cell cycle, including Cyclin E and CDK4/6. Mutations in HRAS, although less common in HNC, can further drive the persistent activation of this proliferative signaling [20].

In addition to RTK-driven pathways, Wnt signaling is another critical oncogenic pathway in HNC. The binding of Wnt ligands to the FZD and LRP5/6 receptors inhibits the destruction complex that normally degrades β-catenin. Stabilized β-catenin accumulates in the nucleus, where it induces the transcription of MYC, Cyclin D1, and JUN, contributing to increased proliferation and survival of cancer cells [21].

The Hippo signaling pathway plays a major tumor-suppressive role by regulating the activity of YAP and TAZ transcription coactivators. Under normal conditions, upstream components of the Hippo pathway, including FAT1, MST1/2, SAV1, and LATS1/2, inhibit YAP/TAZ, preventing them from entering the nucleus. However, mutations or deletions of FAT1 and LATS1/2, which are common in HNC, lead to unchecked YAP/TAZ activation. In the nucleus, YAP/TAZ bind to TEAD1 and stimulate the expression of proliferative genes such as Cyclin D1, MYC, and connective tissue growth factor (CTGF) [22].

Hypoxia, a common feature in solid tumors, further promotes tumor progression in HNC through the stabilization of HIF1A. Under low oxygen conditions, HIF1A induces the expression of VEGFs, which are essential for angiogenesis, ensuring the tumor maintains an adequate blood supply. This supports continued tumor growth and metastasis [23].

Another key driver in HNC is the JAK/STAT3 signaling pathway. Activated by cytokines and growth factors, STAT3 translocates to the nucleus, where it enhances the expression of VEGFs, MYC, Cyclin D1, and other survival genes, promoting immune evasion and sustained tumor growth [24].

Cell cycle progression in HNC is tightly controlled by several key regulators. Cyclin D1 forms a complex with CDK4/6, leading to the phosphorylation and inactivation of the retinoblastoma protein (Rb), which releases E2F transcription factors to induce the expression of Cyclin E and other S-phase genes [8]. Cyclin E reinforces S-phase entry, while MYC supports proliferation by upregulating genes involved in metabolism, ribosome biogenesis, and DNA replication. Activator Protein-1(AP-1) is a transcription factor complex that regulates gene expression in response to various stimuli, including cytokines, growth factors, stress, and bacterial and viral infections. JUN, a component of the AP-1 complex, further enhances proliferation by inducing Cyclin D1 and VEGFs, and it also contributes to invasion through upregulation of matrix metalloproteinases [25].

A. Key oncogenes and activated pathways in HNC

Several components of the HNC network function as oncogenes when mutated or overexpressed, driving uncontrolled growth and survival:

EGFR is overexpressed in up to 90% of HNC cases, promoting persistent activation of downstream PI3K/AKT/mTOR and RAS/RAF/MEK/ERK signaling pathways [26]. FGFR1 amplifications and mutations are reported in 10–15% of HNC cases, contributing to sustained mitogenic signaling [27]. MET amplification and overexpression are observed in 13–21% of cases, enhancing

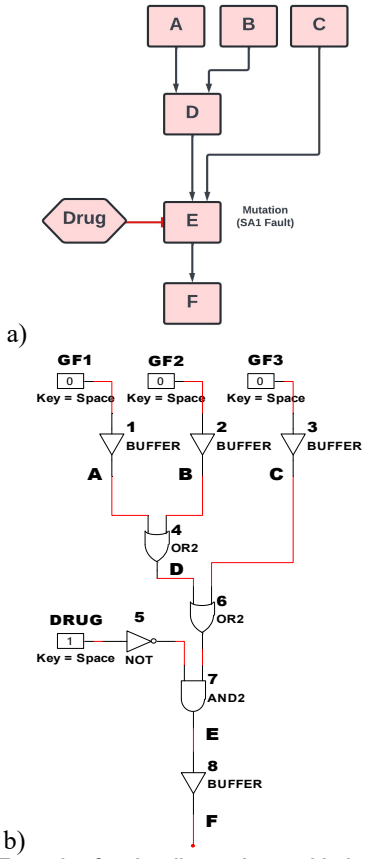

FIGURE 2. (a) Example of a signaling pathway with drug intervention. (b) BN model example of the signaling pathway, with a stuck-at-1 (SA1) fault at gene E, and a drug intervention at gene E to repair the SA1 fault.

invasive and metastatic capabilities [28]. The PI3K/AKT/mTOR pathway is frequently dysregulated in HNC, with alterations occurring in PIK3CA mutations (8.6%), PIK3CA amplifications (14.2%), and PI3K overexpression (27.2%), leading to pathway hyperactivation. [29]. RAS is mutated in 4–6% of HNC cases, leading to constitutive MAPK pathway activation [20]. STAT3 is hyperactivated up to 70% in most of the HNC cases, supporting tumor growth, inflammation, and immune evasion [30]. Aberrant activation of β-catenin through Wnt signaling is less common in HNC but contributes to tumor progression in specific subtypes [31]. YAP/TAZ is activated by the loss of Hippo pathway regulators (e.g., FAT1, LATS1/2), driving transcription of proliferative and anti-apoptotic genes through TEAD [32]. MYC is frequently overexpressed (up to 30% of cases), promoting cell cycle progression and metabolic reprogramming [33]. Cyclin D1 (CCND1) is amplified in approximately 30–40% of HNC cases, leading to dysregulated G1/S phase transition [20]. VEGF is induced by hypoxia (HIF1A), driving angiogenesis to sustain tumor growth [23].

B. Tumor suppressors and their inactivation in HNC

The Frequent loss or mutation of tumor suppressors further drives tumorigenesis:

p53 is mutated in 70–80% of HPV-negative HNC, impairing DNA damage response, apoptosis, and cell cycle

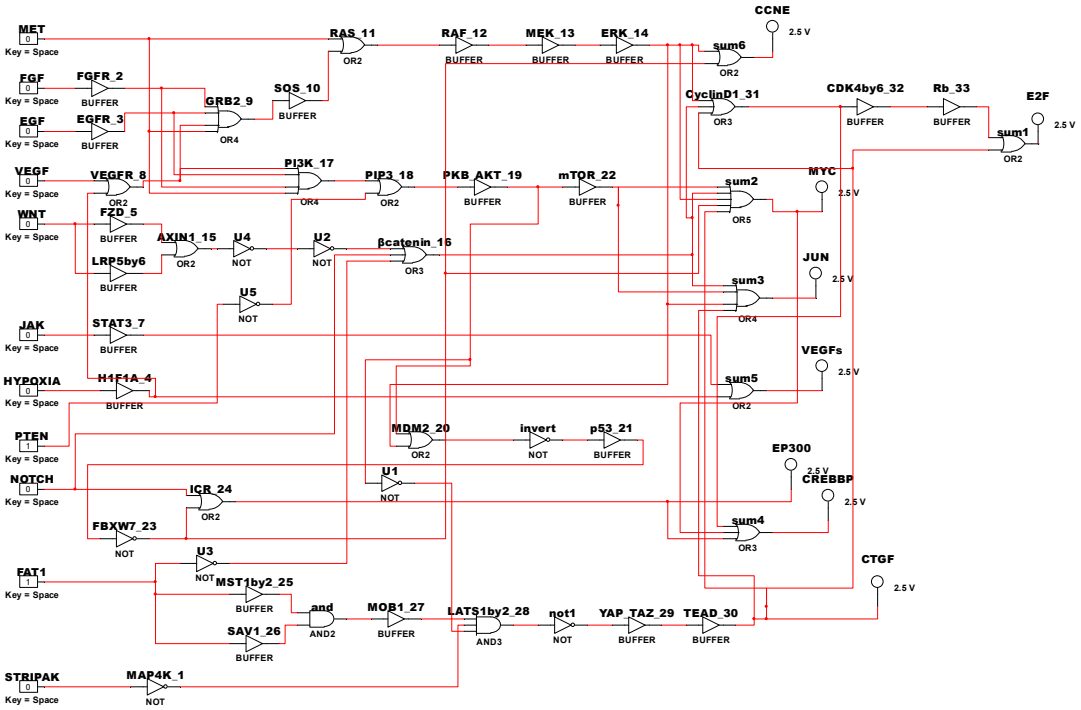

FIGURE 3. Boolean Network model for HNC pathway.

arrest [24]. PTEN loss is observed in 10–15% of cases, leading to constitutive PI3K pathway activation [29]. FBXW7 is mutated in around 5–10% of HNC cases, resulting in the stabilization of oncogenic proteins like Cyclin E and MYC [25]. CREBBP and EP300 are frequently altered epigenetic regulators, mutated or deleted in approximately 10–15% of cases, leading to global transcriptional dysregulation, impaired p53 function, and reduced apoptosis [22]. FAT1 is mutated in 20–30% of HNC cases, resulting in the inactivation of Hippo signaling, enabling unchecked YAP/TAZ activity [22].

III. Methodology

Figure 1 displays the complete biological pathway network for HNC, where the diamond-shaped input nodes represent growth factors, tumor suppressors, receptor tyrosine kinases (RTKs), and transmembrane receptors. The elliptical-shaped nodes on the right side represent reporter genes that serve as outputs for our model design, while the square-shaped nodes in the center represent the interconnected genes and proteins that mediate the signaling interactions throughout the pathway. Solid black arrows in that design represent activation or stimulatory effects, and red lines with hammerhead (T-shaped or blunt endings) represent inhibition or suppressive effects. By mapping these complex molecular interactions within the HNC pathway, we establish a foundation for identifying effective combination therapies, particularly through network-based approaches such as Boolean network modeling. The detailed procedure involved is discussed below.

A. Boolean network modeling of HNC

BNs offer a straightforward and effective approach for modeling cellular signaling pathways, particularly in complex systems like HNC. In this framework, each component of the network, such as a gene or a protein, is represented as a node that exists in one of two possible states: active (on) or inactive (off) [34][35]. This binary abstraction aligns well with the switch-like behavior observed in genetic regulatory networks (GRNs), where genes are either expressed or silenced depending on the cellular context. Within the BN framework, the nodes symbolize genes or signaling molecules, and the edges define the regulatory interactions between them, which can be described through logical functions such as AND, OR, and NOT (Fig. 2).

The Boolean modeling framework operates like a digital logic circuit, where regulatory influences are treated as logic gates that control the activation state of downstream nodes. This enables complex signaling dynamics to be simplified into clear, rule-based relationships. For example, in Fig. 2, our illustrative toy pathway model, if either gene A or gene B activates gene D, this can be represented as an OR logic function, where the presence of either input activates the output. When a single component, such as E, directly activates another component F, without any additional inputs, this is represented through a direct (buffer) connection. Additionally, the drug binding with gene E is modeled using an AND logic gate, where gene D and the drug influence gene E at the same time. By applying this Boolean logic structure across the entire HNC network, we can accurately map intricate molecular interactions into a combinational logic system. This results in a multi-input, multi-output (MIMO) model that captures the complex regulatory architecture of HNC signaling (Fig 3). The ideal (non-proliferative) input and corresponding output states of that system are indicated in Tables I & II, respectively. We used NI Multisim to design all our BN models for this experiment. The Boolean modeling approach used here provides a valuable tool for simulating

TABLE I
INPUTS TO THE HNC BN AND THEIR CORRESPONDING NON-PROLIFERATIVE STATES

Input	Non-proliferative State
MET	0
FGF	0
EGF	0
VEGF	0
WNT	0
JAK	0
HYPOXIA	0
PTEN	1
NOTCH	0
FAT1	1
STRIPAK	0

the effects of drug interventions, identifying potential therapeutic targets, and understanding the global behavior of oncogenic and tumor suppressor pathways within the disease context.

When multiple pathways converge on a common target with potentially conflicting regulatory effects, we assign logical operators based on documented biological behavior. For example, if a target can be activated independently by either gene A or gene B, we modeled this using an OR gate. If activation requires simultaneous input from both, we used an AND gate. In scenarios where upstream signals exert opposing influences (activation vs. inhibition), we applied hierarchical logic, prioritizing the dominant regulatory pathway according to literature evidence. This method aligns with established Boolean network modeling practices and mimics how cells integrate diverse, and sometimes contradictory, signals to make context-dependent decisions.

For computational analysis, both the input and output of the network are expressed as binary row vectors. In this representation, a value of zero (0) signifies an inactive gene, while a value of one (1) represents an active gene. These binary vectors define the activation state of key components within the network, allowing systematic evaluation of how faults and therapies alter the signaling dynamics.

The components of the input vector are given by

Input = [MET, FGF, EGF, VEGF, WNT, JAK, HYPOXIA, PTEN, NOTCH, FAT1, STRIPAK]

while the components of the output vector are given by

Output = [CCNE, E2F, MYC, JUN, VEGFs, EP300, CTGF].

In this study, the input vector is defined as [00000001010], which reflects the absence of external growth signals and the activation of molecular inhibitors, conditions that are expected to produce a non-proliferative output in a fault-free network. Under these normal conditions, the BN generates an output vector of [00000000], indicating controlled cellular behavior with no abnormal proliferation and intact apoptotic processes.

However, when mutations or faults are introduced into the network, applying the same input results in a different, disrupted output, signifying dysregulated signaling that may promote uncontrolled growth or impair apoptosis. The primary goal of therapeutic intervention in this context is to apply drug treatments that shift the faulty output as close as possible to the non-proliferative reference state of [00000000]. From a biological perspective, this involves steering the mutated signaling pathways back towards a regulated, non-proliferative state while reactivating programmed cell death through carefully selected drug combinations.

TABLE II
OUTPUTS OF THE HNC BN (WITHOUT FAULTS) AND THEIR CORRESPONDING NON-PROLIFERATIVE STATES

Output	Non-proliferative State
CCNE	0
E2F	0
MYC	0
JUN	0
VEGFs	0
EP300	0
CREBBP	0
CTGF	0

B. Modeling abnormalities in the HNC pathway

HNC primarily develops because of disrupted cellular signaling, where alterations in normal regulatory pathways lead to the loss of cell cycle control, excessive proliferation, and impaired apoptosis. These abnormalities within the signaling network can be effectively represented in Boolean models as "stuck-at faults," a concept borrowed from digital circuit theory. In this context, a stuck-at fault occurs when a gene or protein node becomes permanently fixed in an active (stuck-at-1) or inactive (stuck-at-0) state, regardless of the upstream signals that would normally regulate its behavior [35]. Such faults may result from genetic mutations, amplifications, deletions, or other structural abnormalities, causing persistent oncogenic activation or loss of tumor suppressor functions. Here, it is important to point out that the stuck-at-fault terminology does have direct clinical relevance to cancer. Stuck-at-1 faults correspond to gain-of-function mutations for oncogenes, while stuck-at-0 faults correspond to loss-of-function mutations for tumor suppressors.

In the case of our BN model for HNC, these faults are used to simulate the effects of common mutations found in the disease. For instance, if a gene like Cyclin D1, which promotes cell cycle progression, becomes constitutively active due to amplification or overexpression, this is modeled as a stuck-at-1 fault. This means that Cyclin D1 continues to drive proliferation regardless of upstream regulatory inputs. Consequently, downstream nodes that control DNA replication and cell division remain persistently activated, contributing to tumor growth. A therapeutic intervention in this scenario might involve the application of CDK4/6 inhibitors, designed to block the downstream effects of Cyclin D1 overactivity and restore controlled cycle progression.

Similarly, the inactivation of critical tumor suppressors in HNC, such as p53 or PTEN, can be modeled as stuck-at-0 faults. Under normal conditions, p53 responds to DNA damage and oncogenic stress by triggering apoptosis or halting the cell cycle [8] [9]. However, when p53 is mutated and loses its function, it becomes permanently inactive, failing to regulate key downstream pathways. This loss contributes to unchecked proliferation, survival, and accumulation of further mutations, accelerating cancer progression. Boolean fault modeling allows us to pinpoint such defects and simulate strategies that might compensate for these losses, such as activating alternative tumor suppressive pathways or using targeted therapies to block the hyperactive oncogenic signals that arise from p53 inactivation.

The stuck-at faults mentioned above directly correspond to common classes of clinical mutations observed in HNC patients. For instance, stuck-at-1 faults represent gain-of-function mutations in oncogenes such as PIK3CA (mutated in 20-25% of HNC cases) or EGFR overexpression (occurring in up to 90% of cases), where the protein becomes constitutively active regardless of upstream regulatory signals. Conversely, stuck-at-0 faults model loss-of-function mutations in tumor suppressors like p53 (mutated in 70-80% of HPV-negative HNC) or PTEN loss (observed in 10-15% of cases), where the protective function is permanently disabled, which can create a synergistic effect that drives aggressive tumor growth [16]. Using the BN, we can explore which drug combinations—such as pairing PI3K inhibitors with mTOR inhibitors—might be most effective in suppressing these cooperative oncogenic signals.

In summary, applying stuck-at fault modeling within a BN offers deep insights into the mutational landscape of HNC. It not only helps in identifying the critical nodes that are driving malignancy but also supports the development of rational, combination-based therapeutic strategies aimed at correcting or bypassing persistent disruptions in the signaling network. By leveraging this system-level understanding, we can work towards more precise and effective treatments tailored to the specific molecular alterations present in each patient's tumor.

C. Simulation for fault mitigation with drug intervention

Using our BN model of HNC, we systematically evaluate various targeted drugs (Table III) combinations to determine their ability to counteract specific genetic and signaling abnormalities, modeled as faults. In this approach, each fault represents a distinct molecular alteration—such as the persistent activation of an oncogene or the loss of a tumor suppressor, reflecting the diverse mutational profiles commonly observed in HNC tumors. The goal is to identify the most effective drug combinations that can neutralize the impact of these faults and restore the network's behavior as closely as possible to its non-proliferative, fault-free state.

To guide this process, we first define the ideal activation patterns of all nodes in a normal, non-mutated network, and these are shown in Tables I and II. When a fault occurs, it alters the output profile of the network, leading to aberrant activity of key genes responsible for cell proliferation, survival, and apoptosis. For each fault scenario, we search for the drug combinations that best correct these abnormal outputs. If complete correction is not possible, we aim to minimize the deviation from the non-proliferative state.

TABLE III
DRUGS AND THEIR RESPECTIVE TARGETS

Drugs	Targets
Cetuximab [36]	EGFR
Erdafitinib [37]	FGFR
Bevacizumab [38]	VEGFR
Buparlisib [39]	PI3K
Capivasertib [40]	AKT
Temsirolimus [41]	mTOR
Ulixertinib [42]	ERK
Ruxolitinib [43]	JAK
Palbociclib [44]	CDK4/6
VT3989 [45]	TEAD
LGK974 [46]	WNT/β-catenin
Vorinostat [47]	FBXW7

To quantify how far a faulted network deviates from the normal state, we use the size difference (SD) score, which measures the difference between the output vectors of the faulted and fault-free networks. Higher SD scores indicate greater activation of proliferative (oncogenic) genes and reduced activity of tumor-suppressive (pro-apoptotic) genes, suggesting a more aggressive cancer phenotype. Therefore, the most effective therapy for each fault is the combination of drugs that produces the smallest SD score, reflecting the greatest restoration of normal signaling, which we discuss in detail in the next subsection.

In our simulations, we also account for the practical aspect of therapeutic application by prioritizing drug combinations that involve fewer agents in order to minimize potential toxicity and adverse effects. To maintain computational efficiency and reflect realistic clinical scenarios, we limit our fault analysis to cases involving up to three simultaneous faulty genes and restrict the therapeutic search space to combinations involving no more than four drugs.

D. Computing the effects of drug combinations

The complete list of FDA-approved or under investigation drugs considered in this study, along with their respective molecular targets within the HNC network, is presented in Table III. To assess the therapeutic potential of these interventions, we systematically analyzed the effects of each drug combination on the network's behavior in the presence of one, two, or three simultaneous faults, representing common genetic mutations and pathway disruptions observed in HNC.

From a systems biology perspective, the BN model of HNC operates similarly to a multi-input, multi-output (MIMO) digital circuit, where the state of the system's outputs is determined by its inputs. In the absence of mutations (the fault-free condition), the BN accurately

reflects the balanced signaling of a non-proliferative cell, producing a stable, controlled output corresponding to regulated proliferation and apoptosis. However, the introduction of faults—such as persistent activation of oncogenes or inactivation of tumor suppressors—disrupts this balance. The resulting output shifts toward an abnormal, cancerous state, mirroring the dysregulated signaling typical of malignant HNC cells.

When non-proliferative input conditions are applied to a faulty network, the output deviates from the ideal, non-proliferative output state due to the effects of these faults. By introducing drugs into this faulty network, the goal is to determine whether the intervention can correct the network behavior, restoring the output closer to the non-proliferative state. To evaluate the effectiveness of each drug or drug combination, we calculate the SD score, a quantitative measure of the difference between the faulty network's output and the fault-free, non-proliferative output.

The specific drugs used in these simulations, listed in Table III, are represented as a row vector of their activity states, as follows:

[Cetuximab, Erdafitinib, Bevacizumab, Buparlisib, Capivasertib, Temsirolimus, Ulixertinib, Ruxolitinib, Palbociclib, VT3989, LGK974, Vorinostat].

This vector format allows us to systematically model the influence of individual drugs or combinations on the overall behavior of the HNC network.

In our BN model for HNC, each element of the drug vector is assigned a binary value of one or zero, indicating whether a specific drug is administered (1) or not (0). As outlined earlier, the primary goal is to guide the output of a faulty network as close as possible to the non-proliferative, non-cancerous output state through targeted drug interventions.

To objectively measure how well a drug or drug combination restores the network toward this ideal state, we use the SD metric. The SD score quantifies the dissimilarity between two binary output vectors—one representing the output of the faulty network and the other representing the non-proliferative, fault-free network. The SD value increases as the difference between these two vectors grows, indicating more severe disruptions to cellular behavior.

Mathematically, SD is calculated by comparing two binary vectors, $a=(a_1,...,a_n)$ and $b=(b_1,...,b_n)$, where each element is either 0 (inactive gene) or 1 (active gene), and 'n' is the length of the vectors. A confusion matrix is constructed to count matches and mismatches across corresponding positions in the two vectors:

$$M = \begin{matrix} \\ b_i = 1 \\ b_i = 0 \end{matrix} \begin{matrix} \begin{matrix} a_i = 1 & a_i = 0 \end{matrix} \\ \begin{pmatrix} A & B \\ C & D \end{pmatrix} \end{matrix} \quad (1)$$

- A: Number of positions where both vectors have a value of 1 (true positives).
- D: Number of positions where both vectors have a value of 0 (true negatives).
- B: Positions where the first vector has a 1 and the second has a 0 (mismatch type 1).
- C: Positions where the first vector has a 0 and the second has a 1 (mismatch type 2).

These counts are then used to calculate the SD score, where higher SD values indicate greater deviation from the non-proliferative state. In biological terms, this suggests a higher degree of abnormal proliferation and reduced apoptosis, both of which are characteristic of aggressive cancer progression. The SD score is given by

$$SD(a,b) = \left(\frac{B+C}{A+B+C+D}\right)^2, \; so\ that\ SD \in [0,1] \quad (2)$$

To assess the effectiveness of each drug combination, we applied our BN across all modeled faults and computed the SD for each scenario. The results of these simulations are organized into a matrix, as shown in Table IV, where each column represents a specific fault, and each row represents a different drug combination. For any given fault, the most effective therapy is identified as the drug combination with the lowest SD value in that column.

TABLE IV
A MODEL NMSD MATRIX: NORMALIZED COMPUTATIONAL EFFECT OF VARIOUS DRUGS IN A BOOLEAN NETWORK MODEL

	Fault 1	**Fault 2**	**Fault 3**	**SD Sum**	**NMSD**
DC1	0.2	0.3	0.6	1.1	0.5
DC2	0.1	0.6	0.7	1.4	0.636
DC3	0.3	0.5	0.8	1.6	0.727
ND	0.5	0.8	0.9	2.2	1.000

To evaluate overall performance across all faults, we sum the SD values across the faults for each drug combination. The combination with the smallest total SD is considered the most effective at globally minimizing the impact of mutations across the network. In Table IV, the first drug combination emerges as the most effective across all three fault locations by achieving the lowest SD sum.

To further explore therapeutic performance under realistic clinical scenarios, we accounted for the occurrence of multiple simultaneous faults, reflecting the complex mutational profiles often observed in HNC. We computed SD scores for all combinations involving one, two, and three concurrent faults within the network. Given the presence of 33 possible fault locations, this resulted in a total of 6,017 fault combinations (calculated as $^{33}C_1 + {}^{33}C_2 + {}^{33}C_3 = 6{,}017$). For each of these fault combinations, we tested the effect of each drug or drug combination and calculated the SD score relative to the non-proliferative output state.

After compiling the full SD matrix for all fault and drug combinations, we normalized the results to ensure comparability and calculated the Normalized Mean Size Difference (NMSD) for each drug. NMSD is a dimensionless value ranging from

0 to 1, where 0 indicates perfect similarity between the outputs (meaning the drug successfully restores non-proliferative behavior), and 1 represents complete dissimilarity (where the drug has no corrective effect). Therefore, a lower NMSD score reflects a more effective therapeutic intervention, while a higher NMSD score suggests that the drug combination is insufficient in counteracting the cancerous signaling caused by the faults.

$$NMSD\ (Drug_i) = \frac{Mean(SD(Drug_i))}{Mean(SD(Untreated))} \quad (3)$$

The NMSD allows us to identify the most effective treatment by comparing the average SD of each drug combination to the average SD of the untreated (fault-only) condition.

A sample NMSD calculation is presented in Table IV, where the most effective drug combination for a specific fault is the one with the lowest SD value. For example, in this case, drug combination 2 (DC2) is the most effective for fault 1, drug combination 1 (DC1) is optimal for fault 2, and drug combination 1 (DC1) again performs best for fault 3. To determine the overall best-performing therapy across all faults, we calculate the NMSD for each drug combination. The combination with the lowest NMSD value is considered the most effective, as it consistently minimizes the impact of mutations across the network. Based on this analysis, drug combination 1 (DC1) demonstrated the greatest overall efficacy in managing the faulty network behavior of HNC.

All BN simulations and NMSD score calculations were implemented in Python, and the complete codebase supporting these analyses is publicly available for reproducibility and further research at the following link: https://github.com/PranabeshTAMU/HNC.

IV. Results and Discussion

With the BN model established in the previous section, we proceed to evaluate the effectiveness of various drug combinations in counteracting specific mutations and pathway malfunctions associated with HNC. For each identified mutation or dysfunction within the network, the primary objective is to determine the most suitable combination therapy capable of minimizing the disruptive effects of the fault and restoring balanced cellular behavior.

For this study, we calculated the NMSD score (as defined in Equation 3) to evaluate the effectiveness of each drug combination applied to the BN model of HNC. The analysis considered cases with one, two, and three simultaneous faults (representing mutations or pathway disruptions). With a total of 12 drugs and limiting the maximum number of drugs in any combination to four, this resulted in 12C1 + 12C2 + 12C3 + 12C4 = 793 possible drug combinations.

Considering the 33 fault locations within the network, the total number of fault scenarios analyzed was $^{33}C_1 + {}^{33}C_2 + {}^{33}C_3 = 6{,}017$ unique fault combinations. The corresponding NMSD matrix generated from this analysis has a dimension of 793 drug combinations by 6,017 fault combinations. Due to the large scale of this dataset, presenting the entire matrix in full is impractical. Instead, we summarized the NMSD scores for all drug combinations across the different fault scenarios, categorized by cases involving single, double, and triple faults. Using the method described previously, the BN simulations were executed in Python, and the complete result is provided in the supplementary materials (see Additional File 1). Some of the top single and two drug combinations are shown in Figs.4 and 5.

In the following subsections, we present the theoretical results obtained from these simulations, alongside corresponding interpretations of the most effective drug combinations identified for managing mutations in HNC.

A. Best treatment strategy for single mutation

We used column charts to illustrate the effectiveness of various drug combinations. VT3989, a TEAD inhibitor, was found to be the most effective single-agent drug with an NMSD score of 0.64 (Table V), showing a 36% reduction compared to untreated conditions. The most effective two-drug combination was Ulixertinib + VT3989, with an NMSD score of 0.33, representing a 67% reduction compared to the untreated case. For three-drug combinations, Ulixertinib + VT3989 + Vorinostat yielded the best results with an NMSD score of 0.17. The most effective four-drug combination was Ulixertinib + VT3989 + LGK974 + Vorinostat, achieving an NMSD score of 0.09, which demonstrates a significant reduction in NMSD score compared to the untreated case.

TABLE V
ROBUST DRUG INTERVENTION STRATEGY
FOR SINGLE MUTATION

Drug Combinations	NMSD
Untreated	1
VT3989	0.6434
Ulixertinib + VT3989	0.3329
Ulixertinib + VT3989 + Vorinostat	0.1733
Ulixertinib + VT3989 + LGK974 + Vorinostat	0.09352

TABLE VI
ROBUST DRUG INTERVENTION STRATEGY
FOR TWO MUTATIONS

Drug Combinations	NMSD
Untreated	1
VT3989	0.692
Ulixertinib + VT3989	0.4203
Ulixertinib + VT3989 + Vorinostat	0.2066
Temsirolimus + Ulixertinib + VT3989 + Vorinostat	0.1187

TABLE VII
ROBUST DRUG INTERVENTION STRATEGY
FOR THREE MUTATIONS

Drug Combinations	NMSD
Untreated	1
Vorinostat	0.7185
VT3989 + Vorinostat	0.4808
Ulixertinib + VT3989 + Vorinostat	0.2423
Temsirolimus + Ulixertinib + VT3989 + Vorinostat	0.1468

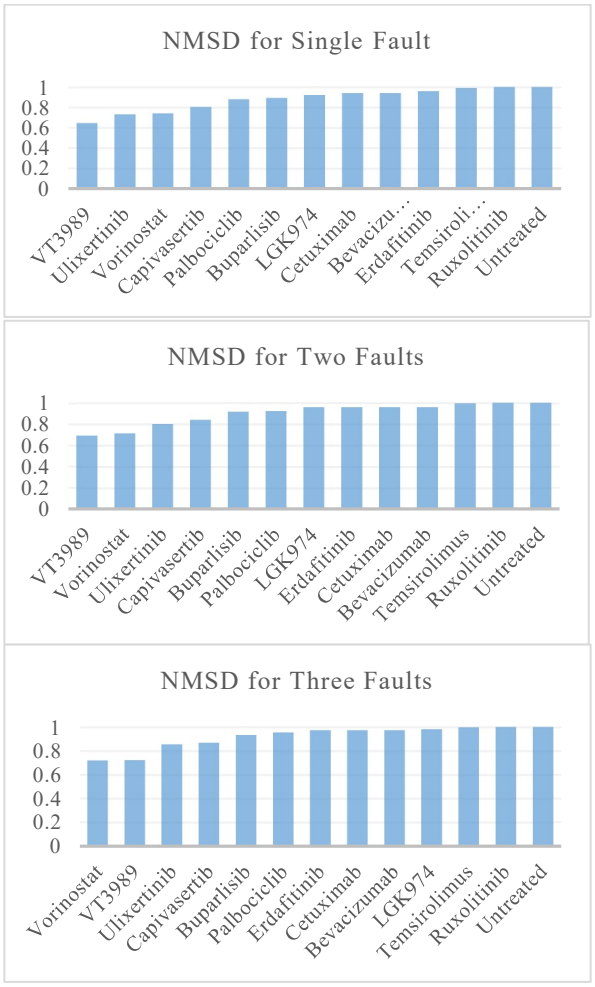

FIGURE 4. All monotherapy drugs (which are used for this experiment), with respective NMSD scores to treat HNC with single, two, and three mutations at a time.

B. Best treatment strategy for two mutations

Similar to the previous subsection, we evaluated drug efficacies for two mutations. As shown in Table VI, VT3989 emerged as the most effective single drug with an NMSD score of 0.69. VT3989 is a nov el TEAD auto palmitoylation inhibitor that targets the Hippo pathway. For two-drug combinations, Ulixertinib + VT3989 proved most effective with an NMSD score of 0.42. The most effective three-drug combination was Ulixertinib + VT3989 + Vorinostat, achieving an NMSD score of 0.21. Finally, the four-drug combination with the lowest NMSD score (0.12) was Temsirolimus + Ulixertinib + VT3989 + Vorinostat.

C. Best treatment strategy for three mutations

In this subsection, we evaluated the best single, two-, three-, and four-drug combinations to treat HNC with three simultaneous mutations. As shown in our analysis, the most effective single drug was Vorinostat, achieving an NMSD score of 0.72. For two-drug combinations, VT3989 + Vorinostat was identified as the most effective, with an NMSD score of 0.48. The best three-drug combination was

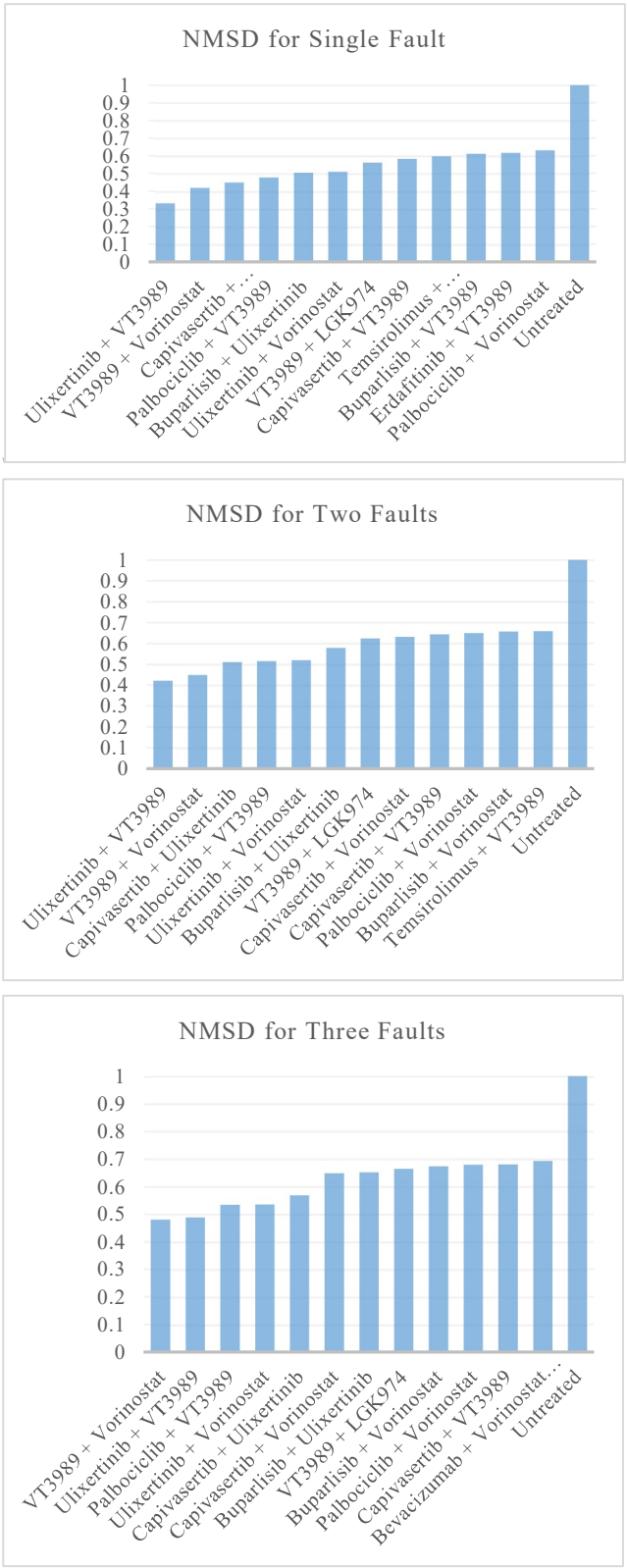

FIGURE 5. Some of the best two-drug combinations with the lowest NMSD score to treat HNC with single, two, and three mutations at a time.

Ulixertinib + VT3989 + Vorinostat, which achieved an NMSD score of 0.24. Finally, the most effective four-drug

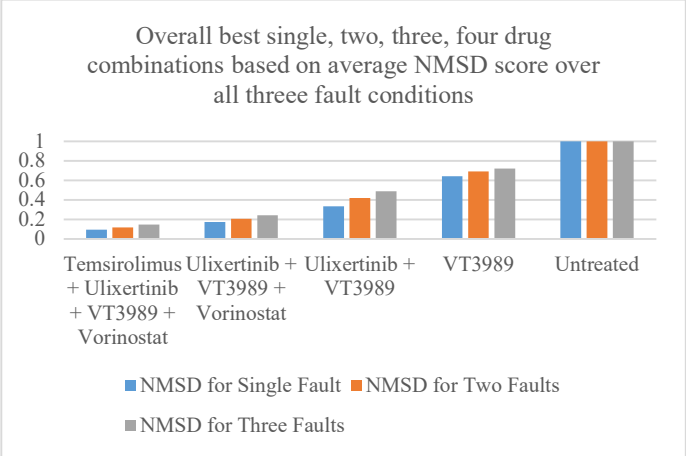

FIGURE 6. Best overall single, two, three and four drug combinations based on average NMSD score.

combination was Temsirolimus + Ulixertinib + VT3989 + Vorinostat, with an NMSD score of 0.15.

D. Best overall drug combinations and analysis of results

The summary of complete simulation results is shown in Fig.6, where the top performing drugs are listed with respective NMSD scores for all single, two and three mutation conditions. In that bar plot we showed the best single, two three and four drug combinations to treat HNC based on lowest average NMSD (mean of single, two and three fault NMSD scores) scores. The results of our simulation provide a comprehensive analysis of targeted therapeutic strategies for HNC, identifying optimal drug combinations based on the NMSD score. The lower the NMSD score, the closer the network dynamics align with a non-proliferative state, making these drug combinations promising candidates for HNC treatment.

Our findings highlight VT3989 as the most effective single-drug th erapy, achieving an average NMSD score of 0.685. VT3989 specifically targets TEAD [45], a key downstream effector of the Hippo signaling pathway, which plays a crucial role in regulating cellular proliferation and apoptosis. TEAD dysregulation in HNC has been associated with tumor progression and therapeutic resistance, suggesting that inhibiting this node can disrupt oncogenic signaling.

For dual-drug therapy, the combination of Ulixertinib + VT3989 demonstrated the highest efficacy, with an average NMSD score of 0.414. Ulixertinib is a potent inhibitor of ERK [42], a critical component of the RAS-RAF-MEK-ERK pathway, which is frequently overactivated in HNC and contributes to uncontrolled cell growth. By simultaneously targeting ERK and TEAD, this combination effectively modulates both proliferative and survival pathways, thereby enhancing therapeutic impact.

Expanding to three-drug regimens, the combination of Ulixertinib + VT3989 + Vorinostat emerged as the top-performing trio, further reducing the NMSD score to 0.207. FBXW7 is an E3 ubiquitin ligase that regulates the degradation of several oncogenic proteins, including MYC, Cyclin E, NOTCH, and mTOR [48]. Some studies suggest that HDAC(histone deacetylase) inhibitor Vorinostat, influences the expression of FBXW7, possibly by altering chromatin accessibility and transcriptional regulation [47]. The addition of Vorinostat potentially enhances the efficacy of Ulixertinib and VT3989 by disrupting compensatory survival mechanisms and reactivating tumor-suppressor pathways.

Finally, the best-performing four-drug combination, Temsirolimus + Ulixertinib + VT3989 + Vorinostat, achieved the lowest average NMSD score of 0.12, indicating a near-complete normalization of pathway dynamics. Temsirolimus, an mTOR inhibitor [41], suppresses PI3K/AKT/mTOR signaling, a key driver of metabolic reprogramming and cell survival in HNC. The inclusion of Temsirolimus likely enhances the therapeutic response by reducing metabolic support for tumor cells, thereby increasing sensitivity to the other three agents.

Our Boolean network model successfully simulates the effects of multiple simultaneous perturbations, as evidenced by our systematic analysis of single, dual, triple, and quadruple drug combinations (793 total combinations tested). The model maintains stability across all perturbation scenarios, with the NMSD metric providing consistent quantitative measures of therapeutic efficacy. The hierarchical improvement in average NMSD scores from single-drug therapy (0.685) to four-drug combinations (0.12) demonstrates that the model can be used to predict the effects of multiple interventions without loss of computational stability.

V. Conclusion and Future Work

In this study, we developed a comprehensive BN model of HNC, incorporating key signaling pathways governing tumor growth, survival, angiogenesis, and apoptosis. By systematically simulating the effects of twelve FDA-approved or under investigation drugs, we identified the most effective single, dual, triple, and quadruple drug combinations based on NMSD scores, which measure the extent to which pathway behavior is restored to a normal state.

It is important to note that Boolean network models, while powerful for systems-level analysis, involve certain abstractions that differ from the continuous and stochastic

nature of biological systems. The binary on/off states used in our model represent simplified versions of the graded protein expression levels and pathway activities observed in real cells. Similarly, the discrete time steps in Boolean networks do not capture the continuous temporal dynamics and varying reaction kinetics of biological processes. Despite these limitations, Boolean models have proven valuable for identifying key regulatory relationships and predicting system-level behaviors, as demonstrated in numerous successful applications in cancer research.

Our findings highlight VT3989 (TEAD inhibitor) as the best-performing single drug, indicating the Hippo pathway as a critical therapeutic target in HNC. The combination of Ulixertinib (ERK inhibitor) + VT3989 significantly improved therapeutic efficacy by simultaneously disrupting the MAPK and Hippo pathways. Further enhancement was observed with the addition of Vorinostat (influences the function of FBXW7, which is a tumor suppressor gene), and Temsirolimus (mTOR inhibitor), which suppresses metabolic adaptation and survival mechanisms. The best four-drug combination, Temsirolimus + Ulixertinib + VT3989 + Vorinostat, achieved the lowest NMSD score, suggesting its potential to comprehensively inhibit tumor-promoting pathways.

VT3989 has shown promising results in clinical trials for patients with advanced malignant mesothelioma and other tumors with specific mutations [49][50][51][52]. The combination of VT3989 with other targeted therapies, such as Ulixertinib (an ERK inhibitor) and Vorinostat (a histone deacetylase inhibitor), likely provides synergistic effects by targeting different but complementary pathways involved in cancer progression. The addition of Temsirolimus, an mTOR inhibitor, to the combination further enhances the multi-targeted approach, potentially addressing multiple cancer-driving pathways simultaneously.

These results underscore the importance of a multi-targeted therapeutic approach in HNC treatment. By simultaneously blocking key oncogenic drivers, our proposed drug combinations have the potential to overcome compensatory resistance mechanisms and improve patient outcomes. This network-based strategy provides valuable insights for precision oncology, offering a rational framework for developing effective combination therapies in HNC.

Collectively, these results underscore the importance of multi-targeted approaches in HNC therapy. The synergistic effects of these drug combinations disrupt multiple oncogenic pathways, minimizing compensatory resistance mechanisms. Our findings suggest that an optimal therapeutic strategy involves the inhibition of TEAD (Hippo pathway), ERK (MAPK pathway), FBXW7 (tumor suppressor), and mTOR (metabolic control), providing a robust framework for precision medicine in HNC treatment. Further experimental validation and clinical translation of these results will be crucial to confirm their efficacy and safety. So, future work will focus on:

a) In Vitro and In Vivo Validation:

- Testing the identified drug combinations in HNC cell lines and patient-derived xenografts (PDX) to validate their efficacy in reducing tumor growth and promoting apoptosis.
- Assessing potential synergistic effects and toxicity profiles of the top-performing drug combinations.
- Correlating experimental results with in silico predictions to confirm the reliability of the Boolean network model in guiding precision therapy decisions.

b) Incorporation of Additional Pathways and Mutations:

- Expanding the BN to include immune checkpoint regulators (e.g., PD-L1, CTLA-4) to evaluate immunotherapy-based combinations [52].
- Investigating the impact of patient-specific mutations to refine treatment strategies for personalized medicine.

c) Clinical Data Integration and Machine Learning Optimization:

- Incorporating HNC patient gene expression and drug response datasets to further validate and refine the model.
- Using machine learning techniques to predict novel drug combinations that may enhance therapeutic efficacy.

By integrating computational modeling with experimental validation, this research paves the way for personalized, data-driven treatment approaches in HNC. The insights gained from this study can serve as a foundation for future clinical trials, ultimately improving therapeutic strategies for HNC patients.

CONFLICTS OF INTEREST

The authors have no competing interests to disclose.

ETHICS STATEMENT

This study does not involve human participants, animals, or clinical trials. It is based solely on Python programming simulations of publicly available pathway diagrams for predictive drug target identification for HNC.

REFERENCES

1. National Foundation for Cancer Research, “Head and Neck Cancers,” NFCR. [Online]. Available: https://www.nfcr.org/cancer-types/cancer-types-head-neck-cancers/. Accessed: 10-Mar-2025.
2. G. R. Ogden, “Head and neck cancer: past, present and future,” British Dental Journal, vol. 233, pp. 889–895, 2022. [Online]. Available: https://www.nature.com/articles/s41415-022-5166-x. Accessed: 10-Mar-2025.
3. A. B. Roberts, C. D. Smith, and E. F. Johnson, “Targeted therapies in head and neck cancer: Advances and future directions,” Frontiers in Oncology, vol. 13, 2023. [Online]. Available: https://pmc.ncbi.nlm.nih.gov/articles/PMC10304137/. Accessed: 10-Mar-2025.
4. American Cancer Society, "ACS Annual Report: Cancer Mortality Continues to Drop Despite Rising Incidence in Women and Young Adults," Jan. 16, 2025. [Online]. Available:

https://pressroom.cancer.org/2025CancerFactsandFigures. Accessed: Mar. 14, 2025.
5. M. Wierzbicka, W. Pietruszewska, A. Maciejczyk, and J. Markowski, “Trends in incidence and mortality of head and neck cancer subsites among elderly patients: A population-based analysis,” Cancers (Basel), vol. 17, no. 3, p. 548, Feb. 2025, doi: 10.3390/cancers17030548.
6. Cancer Research UK, “Head and neck cancers statistics,” Cancer Research UK, 2025. [Online]. Available: https://www.cancerresearchuk.org/health-professional/cancer-statistics/statistics-by-cancer-type/head-and-neck-cancers. Accessed: 10-Mar-2025.
7. S. Marur and A. A. Forastiere, "Head and Neck Squamous Cell Carcinoma: Update on Epidemiology, Diagnosis, and Treatment," Mayo Clin. Proc., vol. 91, no. 3, pp. 386-396, Mar. 2016, doi: 10.1016/j.mayocp.2015.12.017.
8. Leemans CR, Snijders PJF, Brakenhoff RH., "The molecular landscape of head and neck cancer," Nat Rev Cancer, vol. 18, no. 5, pp. 269-282, 2018.
9. Cancer Genome Atlas Network., "Comprehensive genomic characterization of head and neck squamous cell carcinomas," Nature, vol. 517, no. 7536, pp. 576-582, 2015.
10. Sacco AG, Cohen EEW., "Current Treatment Options for Recurrent or Metastatic Head and Neck Squamous Cell Carcinoma," J Clin Oncol, vol. 33, no. 29, pp. 3305-3313, 2015.
11. Vermorken JB, Specenier P., "Optimal treatment for recurrent/metastatic head and neck cancer," Ann Oncol. 21(Suppl 7): vii252–vii261. https://doi.org/10.1093/annonc/mdq453., 2010.
12. Saadatpour A, Albert R., "Boolean modeling of biological regulatory networks: a methodology tutorial," Methods, vol. 62, no. 1, pp. 3-12, 2013.
13. J. Andrews, "Genetics and Molecular Insights into Head and Neck Cancer," Med Clin Oncol., vol. 8, no. 4, pp. 1-10, Dec. 2024. [Online]. Available: https://www.rroij.com/open-access/genetics-and-molecular-insights-into-head-and-neck-cancer.pdf.
14. M. Constantin et al., "Molecular pathways and targeted therapies in head and neck cancers pathogenesis," Front. Oncol., vol. 14, pp. 1373821, Jun. 2024. [Online]. Available: https://www.frontiersin.org/journals/oncology/articles/10.3389/fonc.2024.1373821/full.
15. H. F. Fumiã and M. L. Martins, "Boolean Network Model for Cancer Pathways: Predicting Carcinogenesis and Targeted Therapy Outcomes," PLoS ONE, vol. 8, no. 7, pp. e69008, Jul. 2013. [Online]. Available: https://journals.plos.org/plosone/article?id=10.1371/journal.pone.0069008.
16. Z. Du and C. M. Lovly, "Mechanisms of receptor tyrosine kinase activation in cancer," Molecular Cancer, vol. 17, no. 58, pp. 1-10, Feb. 2018. [Online]. Available: https://molecular-cancer.biomedcentral.com/articles/10.1186/s12943-018-0782-4.
17. H. Zhang et al., "PI3K/AKT/mTOR signaling pathway: an important driver and therapeutic target in triple-negative breast cancer," Breast Cancer, vol. 31, pp. 539-551, Apr. 2024. [Online]. Available: https://link.springer.com/article/10.1007/s12282-024-01567-5.
18. M. W. Ahmed et al., "Expression of PTEN and its correlation with proliferation marker Ki-67 in head and neck cancer," Int J Biol Markers, vol. 31, no. 2, pp. e193-e203, 2016. [Online]. Available: https://journals.sagepub.com/doi/pdf/10.5301/jbm.5000196.
19. T. Knight and J. A. E. Irving, "Ras/Raf/MEK/ERK pathway activation in childhood acute lymphoblastic leukemia and its therapeutic targeting," Front. Oncol., vol. 4, pp. 160, 2014. [Online]. Available: https://www.frontiersin.org/journals/oncology/articles/10.3389/fonc.2014.00160/full.
20. O. Novoplansky et al., "Worldwide prevalence and clinical characteristics of RAS mutations in head and neck cancer: A systematic review and meta-analysis," Front. Oncol., vol. 12, pp. 838911, May 2022. [Online]. Available: https://www.frontiersin.org/journals/oncology/articles/10.3389/fonc.2022.838911/full.
21. A. Sajeev et al., "Crosstalk between non-coding RNAs and Wnt/β-catenin signaling in head and neck cancer: Identification of novel biomarkers and therapeutic agents," ncRNA, vol. 9, no. 5, pp. 63, Oct. 2023. [Online]. Available: https://www.mdpi.com/2311-553X/9/5/63.
22. A. Pocaterra, P. Romani, and S. Dupont, "YAP/TAZ functions and their regulation at a glance," J. Cell Sci., vol. 133, no. 2, pp. jcs230425, Jan. 2020. [Online]. Available: https://journals.biologists.com/jcs/article/133/2/jcs230425/225043/YAP-TAZ-functions-and-their-regulation-at-a-glance.
23. C. Tito et al., "EGF receptor in organ development, tissue homeostasis and regeneration," J. Biomed. Sci., vol. 32, no. 24, pp. 1-10, Feb. 2025. [Online]. Available: https://jbiomedsci.biomedcentral.com/articles/10.1186/s12929-025-01119-9.
24. L. He et al., "YAP and TAZ are transcriptional co-activators of AP-1 proteins and STAT3 during breast cellular transformation," eLife, vol. 10, pp. e67312, Aug. 2021. [Online]. Available: https://elifesciences.org/articles/67312.
25. R. Vartanian et al., "AP-1 regulates Cyclin D1 and c-MYC transcription in an AKT-dependent manner in response to mTOR inhibition: Role of AIP4/Itch-mediated JUNB degradation," Mol. Cancer Res., vol. 9, no. 1, pp. 115-130, Jan. 2011. [Online]. Available: https://aacrjournals.org/mcr/article/9/1/115/90695/AP-1-Regulates-Cyclin-D1-and-c-MYC-Transcription.
26. M. Fasano et al., "Head and neck cancer: the role of anti-EGFR agents in the era of immunotherapy," Therapeutic Advances in Medical Oncology, vol. 13, pp. 1-10, 2021. [Online]. Available: https://journals.sagepub.com/doi/pdf/10.1177/1758835920949418.
27. Y. Bao et al., "Fibroblast growth factor (FGF), FGF receptor (FGFR), and cyclin D1 (CCND1) DNA methylation in head and neck squamous cell carcinomas," Clinical Epigenetics, vol. 13, no. 228, pp. 1-10, Dec. 2021. [Online]. Available: https://clinicalepigeneticsjournal.biomedcentral.com/articles/10.1186/s13148-021-01212-4.
28. S. Hartmann et al., "HGF/Met signaling in head and neck cancer: impact on the tumor microenvironment," Clinical Cancer Research, vol. 22, no. 16, pp. 4005-4013, Aug. 2016. [Online]. Available: https://aacrjournals.org/clincancerres/article/22/16/4005/14946/HGF-Met-Signaling-in-Head-and-Neck-Cancer-Impact.
29. F. E. Marquard and M. Jücker, "PI3K/AKT/mTOR signaling as a molecular target in head and neck cancer," Biochemical Pharmacology, vol. 172, p. 113729, Feb. 2020, doi: 10.1016/j.bcp.2019.113729.
30. Y. Hu et al., "Unraveling the complexity of STAT3 in cancer: molecular understanding and drug discovery," Journal of Experimental & Clinical Cancer Research, vol. 43, no. 23, pp. 1-10, Jan. 2024. [Online]. Available: https://jeccr.biomedcentral.com/articles/10.1186/s13046-024-02949-5
31. D. Javanmard et al., "Investigation of CTNNB1 gene mutations and expression in hepatocellular carcinoma and cirrhosis in association with hepatitis B virus infection," Infectious Agents and Cancer, vol. 15, no. 37, pp. 1-10, Jun. 2020. [Online]. Available: https://infectagentscancer.biomedcentral.com/articles/10.1186/s13027-020-00297-5
32. J. Luo et al., "New insights into the ambivalent role of YAP/TAZ in human cancers," Journal of Experimental & Clinical Cancer Research, vol. 42, no. 130, pp. 1-10, May 2023. [Online]. Available: https://jeccr.biomedcentral.com/articles/10.1186/s13046-023-02704-2.
33. M. F. Zacarías-Fluck et al., "MYC: there is more to it than cancer," Frontiers in Cell and Developmental Biology, vol. 12, pp. 1342872, Mar. 2024. [Online]. Available: https://www.frontiersin.org/journals/cell-and-developmental-biology/articles/10.3389/fcell.2024.1342872/full.
34. M. Mondal, A. Lahiri, H. Vundavilli, G. d. Priore, N. P. Reeves and A. Datta, "A Computational Study of Efficient Combinations of FDA-Approved Drugs and Dietary Supplements in Endometrial Cancer," in IEEE Access, vol. 12, pp. 190746-190759, 2024, doi: 10.1109/ACCESS.2024.3503438.
35. A. Lahiri, H. Vundavilli, M. Mondal, P. Bhattacharjee, B. Decker, G. Del Priore, N. P. Reeves, and A. Datta, "Drug target identification in triple negative breast cancer stem cell pathways: A computational study of gene regulatory pathways using boolean networks," IEEE Access, vol. 11, pp. 56672-56690, 2023.
36. J. Zhou, Q. Ji, and Q. Li, "Resistance to anti-EGFR therapies in metastatic colorectal cancer: underlying mechanisms and reversal strategies," J. Exp. Clin. Cancer Res., vol. 40, no. 328, 2021.

37. S. Lim et al., "Antiangiogenic activity of FGFR inhibitor erdafitinib in urothelial carcinoma," Cancer Res., vol. 82, no. 12_Supplement, 2022.
38. F. Kazazi-Hyseni, J. H. Beijnen, and J. H. M. Schellens, "Bevacizumab," The Oncologist, vol. 15, no. 8, pp. 819-825, 2010.
39. [39] A. C. Garrido-Castro et al., "Phase 2 study of buparlisib (BKM120), a pan-class I PI3K inhibitor, in patients with metastatic triple-negative breast cancer," Breast Cancer Res., vol. 22, no. 120, 2020.
40. L. M. Smyth et al., "Capivasertib, an AKT kinase inhibitor, as monotherapy or in combination with fulvestrant in patients with AKT1E17K-mutant, ER-positive metastatic breast cancer," Clin. Cancer Res., vol. 26, no. 15, pp. 3947-3957, 2020.
41. B. I. Rini, "Temsirolimus, an inhibitor of mammalian target of rapamycin," Clin. Cancer Res., vol. 14, no. 5, pp. 1286-1290, 2008.
42. R. Sigaud et al., "The first-in-class ERK inhibitor ulixertinib (BVD-523) shows activity in MAPK-driven pediatric low-grade glioma models as single agent and in combination with MEK inhibitors or senolytics," Neuro-Oncology, vol. 24, no. Supplement_1, p. i93, 2022.
43. E. Senkevitch et al., "The JAK inhibitor ruxolitinib is effective in treating T cell acute lymphoblastic leukemia with gain of function mutations in IL-7R alpha," Blood, vol. 126, no. 23, p. 1330, 2015.
44. M. H. O'Hara et al., "Phase II study of palbociclib in patients with tumors with CDK4 or CDK6 amplification: Results from the NCI-MATCH ECOG-ACRIN trial (EAY131) subprotocol Z1C," Clin. Cancer Res., vol. 31, no. 1, pp. 56-64, 2025.
45. T. T. Tang and L. Post, "VT3989, the first-in-class and first-in-human TEAD auto-palmitoylation inhibitor, enhances the efficacy and durability of multiple targeted therapies of the MAPK and P13K/AKT/mTOR pathways," Mol. Cancer Ther., vol. 22, no. 12_Supplement, 2023.
46. J. Liu et al., "Targeting Wnt-driven cancer through the inhibition of Porcupine by LGK974," Proceedings of the National Academy of Sciences, vol. 110, no. 50, pp. 20224–20229, Dec. 2013. [Online]. Available: https://www.pnas.org/doi/10.1073/pnas.1314239110. Accessed: 10-Mar-2025.
47. S. Duvic and M. Zhang, "Vorinostat: A new oral histone deacetylase inhibitor approved for cutaneous T-cell lymphoma," Expert Opinion on Investigational Drugs, vol. 16, no. 7, pp. 1111–1120, Jul. 2007. [Online]. Available: https://pubmed.ncbi.nlm.nih.gov/17594151/. Accessed: 10-Mar-2025.
48. A. Yeh, "FBXW7: a critical tumor suppressor of human cancers," Molecular Cancer, vol. 17, no. 1, pp. 1-19, 2018. [Online]. Available: https://molecular-cancer.biomedcentral.com/articles/10.1186/s12943-018-0857-2.
49. T. A. Yap et al., "First-in-class, first-in-human phase 1 trial of VT3989, an inhibitor of yes-associated protein (YAP)/transcriptional enhancer activator domain (TEAD), in patients with advanced solid tumors enriched for malignant mesothelioma and other tumors with neurofibromatosis 2 (NF2) mutations," presented at the AACR Annual Meeting 2023, Apr. 2023. [Online]. Available: https://www.onclive.com/view/vt3989-shows-activity-tolerability-in-mesothelioma-and-other-nf2-mutated-solid-tumors.
50. The ASCO Post, "VT3989 May Be Safe, Effective in Patients with Advanced Mesothelioma and NF2-Mutant Solid Tumors," Apr. 2023. [Online]. Available: https://ascopost.com/news/april-2023/vt3989-may-be-safe-effective-in-patients-with-advanced-mesothelioma-and-nf2-mutant-solid-tumors/.
51. Clinical Trials Arena, "Vivace Therapeutics reports positive results for NF2 tumour drug," Apr. 2023. [Online]. Available: https://www.clinicaltrialsarena.com/news/vivace-therapeutics-mesothelioma-nf2/.
52. M. Proctor, E. Suvernev, and A. Dobrovolskiy, "Modelling of Immune Checkpoint Network Explains Synergistic Anti-CTLA-4 and Anti-PD-1 Immunotherapy," Frontiers in Immunology, vol. 11, p. 1880, 2020. [Online]. Available: https://www.frontiersin.org/articles/10.3389/fimmu.2020.01880/full.